Supplementary Data

Supplementary Methods

The following comprehensive explanation of the numerical simulations may accord with information already given in the original paper, in order to guaranty that the relevant context is addressed.

Numerical Simulations

The objective of the simulations was to ascertain the influence on risk of EMI of different lead placements, heart positions in the thorax and tissue conductivities of the organs by numerically calculating the voltage induced in bipolar leads. We therefore used two kinds of human models: A XCAT-male model (cf. Figure S1 panel a and b) and a simplified body model (cf. Figure S1 panel c and d).

The XCAT-male model was developed by Simpleware Ltd. in the ScanIP+FE software environment using the XCAT phantom data set from Duke University.[1-3] It represents the 50th percentile US adult male (height: 1.76 m, weight: 81 kg, BMI=26) with precise organ, bone and muscle structures in the upper body. The organs, bones and muscles were all assigned with their specific tissue properties, i.e. electrical conductivity and relative permittivity given by Hasgall et al. and the standard IEC 62226-3-1.[4,5] The detailed values are listed in Table S2. Thus, the XCAT-male model enables real case simulations.

The simplified body model consisted of 26 basic 3-dimensional solids like cubes, spheres and cylinders. The model's physique (e.g. height, weight, chest circumference) were taken from Bargmann et al.[6] The model's height was set to 1.7 m and its weight to 70.5 kg (BMI=24). The advantage of the simplified body model is that model size, organ positions and tissue

properties can be freely modified. For validation, the results of the simplified body model were compared with the real case simulations of the XCAT-male model.

The numerical simulations were executed separately for electric and magnetic fields. The magnetic field was applied perpendicular to the frontal plane of the human model with homogenous flux density of 1 mT. The electric field was applied perpendicular to the transverse plane of the human model with homogenous field strength of 1 kV/m. For electric and magnetic fields the simulated field frequency was set to 50 Hz. This simulation approach represents worst-case exposure and is therefore consistent with the setup of the in vivo provocation studies.[7] The results of the numerical simulations can thus be applied to the data of the *in vivo* provocation studies.

Influence of the Lead-Tip's Position and Orientation

The voltage induced in the distal end of bipolar leads depends on the current which forms inside a human body when exposed to electric or magnetic fields. This current is generally specified as current density and varies in magnitude and direction within the human model due to the shape and the different tissue properties of the organs. Therefore the current density distribution due to the electric or the magnetic field is a property of the human models.

In case of electric fields the distribution of the induced current density in the thorax is shown in Figure S2 panel a. The general direction of the current density vectors points vertically from cranial to caudal. In the upper thorax region the vectors tend to point to the heart. This is due to the current's attraction to volumes of higher conductivity on their path down to the grounded feet. The current density between the lungs increases in caudal direction.

In case of magnetic fields (cf. Figure S2 panel b) the direction of the induced current density in the thorax is pointing cranial on the right and caudal on the left body side (clockwise

rotation). Along the transverse axis the current density is increasing from central to lateral body parts.

To scrutinize how the current density distribution determines the induced voltage and therefore the influence of lead placement on risk of EMI we numerically implemented the distal end of the lead (lead-tip) with a tip and a ring electrode within the heart and a tip-to-ring spacing of 10 mm. We then changed the position and the orientation of the lead-tip.

The influence of lead-tip's position was evaluated in the apex of the XCAT-male's right ventricle (P_V cf. Figure S1, panel b) and in seven different positions within the heart of the simplified body model (P_1 to P_7 cf. Figure S1, panel d). P_1 is the heart's center and all other positions are shifted (3 cm) along the frontal, transverse and longitudinal axis.

The influence of lead-tip's orientation was evaluated at each position (P_V, P_1-P_7) by rotating the ring electrode around the tip electrode between 0° and 180° in 10° steps in all three anatomical planes (frontal, transverse, sagittal). The tip electrode is thereby held in the transverse plain (colored grey in Figure S2 panel c and d)

Influence of the Heart Position

To determine the influence of the heart position in the thorax on risk of EMI we scrutinized four different positions in the simplified body model which represent individual heart positions. The 1st position (H1) is shown in Figure S1 where the heart model (colored blue) is in the initial position. For the 2nd position (H2) the heart was moved up 10 cm along the longitudinal axis. For the 3rd position (H3) the heart was moved down 4 cm along the longitudinal axis and for the 4th position (H4) the heart was moved down 5 cm and 4 cm to the left along the transverse axis. At each heart position the lung was of course remodeled accordingly.

Influence of the Tissue Conductivity

The tissue conductivities of the organs influence the induced voltage and therefore affect the risk of EMI. As they are individual different and can vary over time we assigned four different conductivity sets to the body (σ_b), the blood in the heart (σ_h) and the lung (σ_l) in the simplified body model.[5,8-11] The values of the conductivity sets (CS1-CS4) are listed in Table S3. The assigned relative permittivity was chosen according to Hasgall et al. and IEC 62226-3-1.[4,5] The assigned relative permeability (μ_r) equals to one in all cases.

Determining the Induced Voltage

The induced voltage was determined with respect to the lead-tip's orientation for all lead–tip's positions (P_V, P_1-P_7), heart positions (H1-H4) and tissue conductivities (CS1-CS4) – in total 113 separate simulations. As shown in Figure S2 (panel c and d) the induced voltage can be mapped on a quarter sphere where the center represents the tip electrode and the lead-tip's orientation determines the ring position on the shell of the sphere. Thus, the angle between the transverse plane and a straight line connection from tip to ring electrode determines the portion of the maximum induced voltage. This angle is further referred to as polar angle θ. For every orientation (θ=0° to 180° in the three anatomical planes) the induced voltage due to the electric field (V_E) and the magnetic field (V_B) were numerically calculated. The numerical calculations were done using Equation 3 and Equation 4 (cf. the following sections "Numerical Implementation of the Electric Field Exposure" and "Numerical Implementation of the Magnetic Field Exposure").

Numerical Implementation of the Electric Field Exposure

A vertically polarized 50 Hz homogeneous electric field with field strength of 1 kVm^{-1} (E_0) was simulated. The distribution of the current density was calculated with ANSYS Solver "Solid232". Solid232 calculates the conduction current density ($\vec{J}_{cE}(x,y,z)$) and the

displacement current density ($\vec{J}_{dE}(x,y,z)$) induced by an exogenous electrical field for every knot of the mesh.

The electric potential difference between T (location of the tip-electrode) and R (location of the ring-electrode) within the model equals the total induced voltage due to the exogenous electric field (V_E). It is given by Equation 1.

$$V_E = V_T - V_R = \int_R^T \vec{E}_E d\vec{s} \qquad \text{Equation 1}$$

$\vec{E}_E$ is the electric field inside the model which is induced by the exogenous electric field. $\vec{E}_E$ can be calculated using Equation 2.

$$\left|\vec{J}_E\right| = \left|\vec{J}_{cE} + \vec{J}_{dE}\right| = \sqrt{\sigma^2 + (\omega\varepsilon_0\varepsilon_r)^2}\, E_E \qquad \text{Equation 2}$$

For the numeric implementation we derived Equation 3.

$$V_E = \sum_{n=2}^{N} \frac{\vec{E}_E(n-1) + \vec{E}_E(n)}{2} ds \qquad \text{Equation 3}$$

N is the number of points on the path form R to T where $\vec{E}_E$ was calculated. ds is the distance between two consecutive points on the path.

Numerical Implementation of the Magnetic Field Exposure

Because the relative permeability (μ_r) is approximately the same for the human body and the air exogenous volumes can be neglected for the magnetic field simulation. Therefore the boundary conditions (the magnetic scalar potential) were assigned directly to models surface. The scalar potential drives a homogeneous magnetic field in z-direction (sagittal) with a flux density of 1 mT. The solver "Solid236" was used to calculate the induced conduction current density ($\vec{J}_{cB}(x,y,z)$) and the displacement current density ($\vec{J}_{dB}(x,y,z)$). The total induced

voltage due to the exogenous magnetic field (V_{BDis}) is then calculated in the same way as V_{EDis}. For the numeric implementation we derived Equation 4.

$$V_B = \sum_{n=2}^{N} \frac{E_B(n-1) + B_B(n)}{2} ds \qquad \text{Equation 4}$$

Here V_B equals the induced voltage due to the eddy currents (V_{BDis}) induced in the human model by the magnetic field.

Supplementary Results

Influence of Tissue Conductivity, Lead-Tip's and Heart Position on the Risk of EMI

The influence of tissue conductivity, lead-tip's position as well as heart position on the risk of EMI was evaluated using the simplified body model. Table S4 provides a comparison of the induced voltage of all scrutinized tissue conductivities (CS1-CS4) and heart positions (H1-H4) for the electric field. The results are normalized to the maximum induced voltage (V_{EMax}) at H1 and CS1. If one reads Table S4 row wise the effect of changing the heart position in the thorax can be evaluated. A vertical or horizontal movement of the heart reduces the induced voltage. Overall, the induced voltage changed only about 16% at maximum between the different heart positions (not comparing different conductivity sets). If one reads Table S4 column wise it is recognizable that V_{EMax} is decreasing when the tissue conductivity increases.

Table S5 provides a comparison of the induced voltage of all scrutinized tissue conductivities (CS1-CS4) and heart positions (H1-H4) for the magnetic field. The results are normalized to the maximum induced voltage (V_{BMax}) at H1 and CS1. Increasing the conductivity of the body (σ_b) increases V_{BMax} (cf. CS1 and CS3). Increasing the conductivity of the heart (σ_h) decreases V_{BMax} (cf. CS1 and CS2). Shifting the heart 4 cm along the transverse axis from the

body center towards the lateral ribs drastically increased the maximum induced voltage V_{BMax} by 219% (cf. H3 and H4). Whereas a 10 cm vertical shift of the heart towards cranial reduced the induced voltage only slightly by 22% (cf. H1 and H2).

Results for different lead-tip's positions within the heart are addressed by Table S6 and described in more detail in the main manuscript.

Supplementary Tables

Table S1 Patient characteristics (n = 160). Data are expressed as the mean value ± SD (range) when appropriate

Male/female, number (%)	124 / 36 (77.5 / 22.5)
Age [years]	59.7 ± 12.0 (21 - 79)
Height [cm]	174.7 ± 9.4 (141 - 198)
Weight [kg]	84.2 ± 15.4 (49 - 129)
Body mass index [$kg*m^{-2}$]	27.5 ± 4.3 (19 - 42)
Circumference of thorax [cm]	104.4 ± 9.5 (76 - 129)
Circumference of abdomen [cm]	102.3 ± 12.5 (65 - 134)
Circumference of hip [cm]	104.8 ± 9.6 (83 - 138)
Circumference of upper arm [cm]	31.7 ± 3.7 (20 - 46)
Distance between the shoulders [cm]	42.8 ± 6.5 (26 - 64)
Diameter of heart [cm]	16.5 ± 2.2 (11 - 22)
Diameter of thorax [cm]	32.7 ± 2.8 (26 - 38)
ICD / PM, number *	81 / 79

ICD, implantable cardioverter-defibrillator; PM, pacemaker.

Table S2 Tissue properties of the XCAT-male model.[4,5]

Body part name	**Conductivity**	**Relative permittivity**
Bulk	0.2000	10000
Bone	0.0807	788913.33
Muscle	0.2334	17718930.33
Cartilage	0.1714	1637727.69
Lung (inflated)	0.0684	5758909.75
Lung (deflated)	0.2054	868583.74
Oesophagus (Air)	2.5e-14	1
Trachea (Air)	2.5e-14	1
Liver	0.0367	1831716.19
Stomach (lumen)	0.2334	17718930.33
Spleen	0.0857	10188454.18
Pancreas	0.5214	1637692.25
Kidney	0.0892	10114814.32
Gall Bladder	0,9000	1449.43
Diaphragm	0.2333	17718930.33
Blood	0.7000	5259,91
Myocardium	0.0827	8664566.37

Table S3 Sets of conductivities assigned to the simplified body model [5,8-11]

Set Name	σ_b $[S/m]$	σ_h $[S/m]$	σ_l $[S/m]$
S1	0.2	0.5	0.15
CS2	0.2	0.7	0.15
CS3	0.5	0.7	0.15
CS4	0.5	1.0	0.15

Table S4 Results of the maximum induced voltage for the electric field ($\boldsymbol{V_{EMax}}$) for all tissue conductivities and heart positions. The results are normalized to heart positions H1 with the tissue conductivity of CS1 acquired at P_1 in the frontal plane.

Heart position	$\boldsymbol{V_{EMax}}$ **with CS1[%]**	$\boldsymbol{V_{EMax}}$ **with CS2[%]**	$\boldsymbol{V_{EMax}}$ **with CS3[%]**	$\boldsymbol{V_{EMax}}$ **with CS4[%]**
H1	100.0	79.72	65.59	52.89
H2	85.16	68.03	54.83	44.20
H3	100.9	80.58	64.93	52.76
H4	97.45	76.88	52.28	41.16

Table S5 Results of the maximum induced voltage for the magnetic field ($\boldsymbol{V_{BMax}}$) for all tissue conductivities and heart positions. The results are normalized to heart position H1 with the tissue conductivity of CS1 acquired at P_1 in the frontal plane.

Heart position	$\boldsymbol{V_{BMax}}$ **with CS1[%]**	$\boldsymbol{V_{BMax}}$ **with CS2[%]**	$\boldsymbol{V_{BMax}}$ **with CS3[%]**	$\boldsymbol{V_{BMax}}$ **with CS4[%]**
H1	100.0	81.8	126.3	103.3
H2	78.2	63.6	84.2	68.3
H3	112.2	92.4	186.0	154.4
H4	318.8	252.1	357.9	284.4

Table S6 The results for the maximum current densities within the heart for different positions of the lead-tip. P_V refers to the XCAT-male model and P_1-P_7 refer to the simplified body model (with CS1).

Current density due to:	**P_V / P_1, P_5, P_6** [mA/m^2]	**P_3** [mA/m^2]	**P_2** [mA/m^2]	**P_4,P_7** [mA/m^2]
Electric Field	6.0	6.1	5.7	6.1
Magnetic Field	3.7	2.6	7.4	3.6

Supplementary Figures

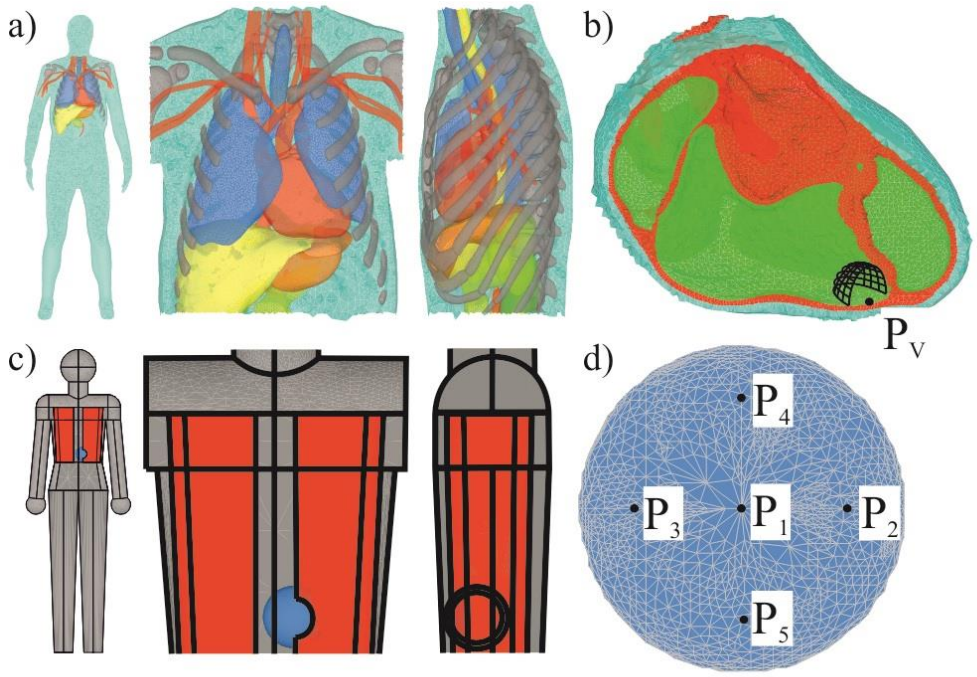

Figure S1 Panel a: The XCAT-male and a close up of its thorax in frontal and lateral view. Panel b: Cross-section image of the XCAT-male's heart. The myocardium is colored red and the chambers green (right atrium, right ventricle, left ventricle). The examined position of the tip electrode is indicated with P_V. Panel c: the simplified body model and a close up of its thorax in frontal and lateral view. The heart is colored blue and located in position H1. Panel d: Cross-section image of the heart of the simplified body model. Indicated are five of seven different positions (P_1 to P_5) of the lead-tip which were investigated.

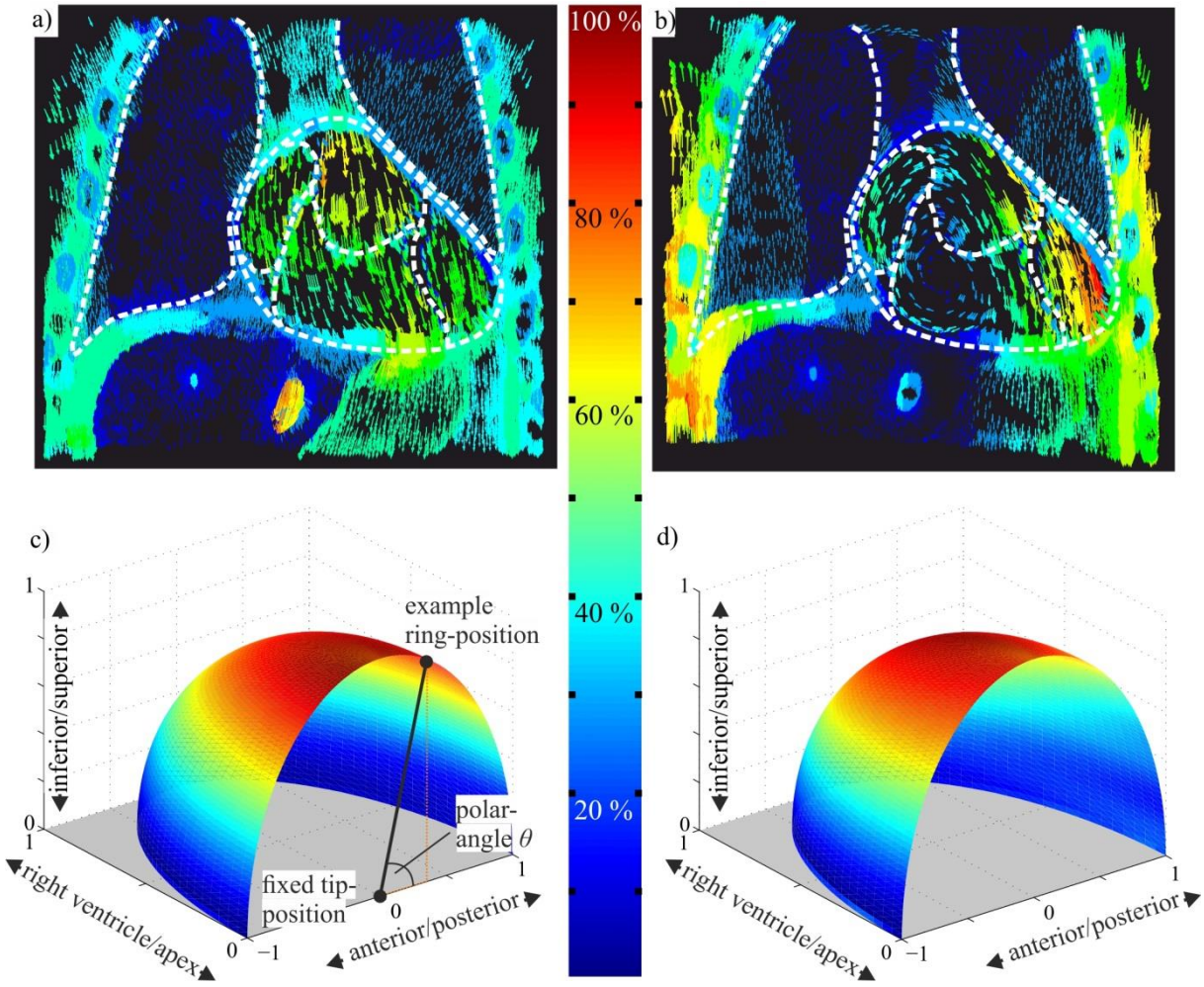

Figure S2 Current density distribution in the thorax (frontal plane) of the human model. Shown here for the XCAT-male model. In panel a: for the electric field and in panel b for the magnetic field. The color scales in the middle indicates the portion of the current density. The maximum current density was scaled to 100%. Panel c and d: the induced voltage for all orientations of the lead-tip can be mapped on a quarter sphere. Shown here for P_V (cf. Figure S1) of the XCAT-male model. The color at a certain point on the sphere indicates the portion of the maximum induced voltage for the corresponding polar angle (θ) from 100% (red) to 0% (blue). Panel c: the voltage induced by an electric field (V_E). As an example a lead-tip (tip and ring electrode) and the corresponding polar angle θ is indicated. Panel d shows the equivalent quarter sphere of the induced voltages due to the magnetic field (V_B) for any orientation of the lead-tip.

Supplementary References

1. Segars WP, Bond J, Frush J, Hon S, Eckersley C, Williams CH, et al. Population of anatomically variable 4D XCAT adult phantoms for imaging research and optimization. Med Phys 2013; 40:043701.
2. Segars WP, Sturgeon G, Mendonca S, Grimes J, Tsui BM. 4D XCAT phantom for multimodality imaging research. Med Phys 2010; 37:4902-15.
3. Genc KO, Segars P, Cockram S, Thompson D, Horner M, Cotton R, et al. Workflow For Creating a Simulation Ready Virtual Population For Finite Element Modeling. Journal of Medical Devices 2013; 7:040926-.
4. IT'IS Database for thermal and electromagnetic parameters of biological tissues [Internet]. Version 2.5, August 1st 2014. Available from: www.itis.ethz.ch/database.
5. IEC62226-3-1:2008-06. Exposure to electric or magnetic fields in the low and intermediate frequency range - Methods for calculating the current density and internal electric field induced in the human body - Part 3-1: Exposure to electric fields - Analytical and 2D numerical models. 2008.
6. Bargmann W, Leonhardt H, Töndury D. Lehrbuch und Atlas der Anatomie des Menschen. 20 ed. Töndury G, editor. Stuttgart: Georg Thieme Verlag; 1968.
7. Napp A, Joosten S, Stunder D, Knackstedt C, Zink M, Bellmann B, et al. Electromagnetic interference with implantable cardioverter-defibrillators at power frequency: an in vivo study. Circulation 2014; 129:441-50.
8. Gabriel C, Gabriel S, Corthout E. The dielectric properties of biological tissues: I. Literature survey. Phys Med Biol 1996; 41:2231-49.
9. Gabriel C, Peyman A, Grant EH. Electrical conductivity of tissue at frequencies below 1 MHz. Phys Med Biol 2009; 54:4863-78.

10. Gabriel S, Lau RW, Gabriel C. The dielectric properties of biological tissues: II. Measurements in the frequency range 10 Hz to 20 GHz. Phys Med Biol 1996; 41:2251-69.
11. Gabriel S, Lau RW, Gabriel C. The dielectric properties of biological tissues: III. Parametric models for the dielectric spectrum of tissues. Phys Med Biol 1996; 41:2271-93.